

# Counterpropagating dipole-mode vector soliton

Jochen Schröder, Philip Jander, and Cornelia Denz

*Institute of Applied Physics, Westfälische Wilhelms-Universität Münster, D-48149 Münster, Germany*

Tobias Richter, Kristian Motzek, and Friedemann Kaiser

*Institute of Applied Physics, Darmstadt University of Technology, D-64289 Darmstadt, Germany*

Received October 26, 2004

We experimentally observed a counterpropagating dipole-mode vector soliton in a photorefractive SBN:60Ce crystal. We investigated the transient formation dynamics and show that the formation process differs significantly from the copropagating geometry. The experimental results are compared with fully anisotropic numerical simulations and show good qualitative agreement. © 2005 Optical Society of America  
 OCIS codes: 190.5530, 190.5330.

Spatial optical solitons in a counterpropagating (CP) geometry were proposed some time ago.<sup>1</sup> It was not until recently, however, that they have drawn wide attention<sup>2–5</sup> and were investigated theoretically in saturable Kerr and local photorefractive media in one transverse dimension. In addition, Cohen *et al.* experimentally demonstrated the existence of stable CP solitons with narrow stripe beams.<sup>3</sup>

Previously, the existence of stable two-dimensional higher-order CP vector solitons in saturable Kerr media that are commonly used as an approximation for photorefractive nonlinearity was predicted.<sup>6</sup> Here we experimentally and numerically demonstrate the existence of a CP dipole-mode vector soliton in a photorefractive SBN:60Ce crystal and investigate the transient formation dynamics.

A dipole-mode vector soliton consists of two mutually incoherent beams: an optical dipole and a fundamental-mode (FM) beam. The individually propagating dipole does not form a spatial soliton owing to repulsion of the dipole components.<sup>7,8</sup> However, if a FM beam that is incoherent to the dipole is launched between the dipole components, they will be trapped by means of incoherent attraction.<sup>7,9</sup>

The CP geometry poses some additional challenges to the experimental setup. A soliton propagating inside a photorefractive crystal will be displaced in the positive direction of the crystal's *c* axis. This effect is well known as the so-called beam-bending effect caused by charge-carrier diffusion. This effect has been extensively investigated for single-soliton formation. For interacting copropagating solitons or copropagating vector solitons the effect does not change the fundamental interaction behavior, as the beams are displaced by the same amount.<sup>10</sup> Two CP solitons, however, are bent in the same direction. Thus, when they are launched in a head-on configuration, they will cross inside the crystal, resulting in a change of the soliton interaction length. Therefore beam bending has a significant effect on transient formation dynamics, as will become apparent below. Although at a first, rough glance the CP geometry might be quite similar to configurations for, e.g., double phase conjugate mirrors, in experiments the two are in fact quite distinct. The two interacting beams are mutually incoherent and thereby do not interfere in the material.

The lack of an interference grating is obvious because of the insensitivity of the beams to slight angular changes once the solitons are formed. This effect can be seen directly when one is observing the dynamics of the soliton formation. By contrast, the existence of a grating would result in a highly selective Bragg condition. Such behavior is typical for double phase conjugation configurations but does not appear in our case. Moreover, the scales are much smaller than for double phase conjugate experiments (input beams are  $\sim 20 \mu\text{m}$ ; interaction angles are smaller than  $1^\circ$ ), and effects that are typically associated with four-wave mixing and phase conjugation do not appear on that scale. Nevertheless, in all our experiments we checked thoroughly to ensure that the effects that we were observing were indeed caused by CP solitons.

The experimental setup is depicted in Fig. 1. A frequency-doubled Nd:YAG laser beam is divided into two beams. These beams are rendered mutually incoherent by means of a piezo-driven mirror oscillating much faster than the response time of the crystal and are then focused onto the two faces of the photorefractive SBN crystal by two beam splitters. Because of the mutual incoherence of the beams, they do not interfere in the material or produce an interference grating, thereby interacting only by means of their common phase modulation and induced refractive-index channel. The crystal is biased with an external dc field along the *x* axis parallel to the crystallo-

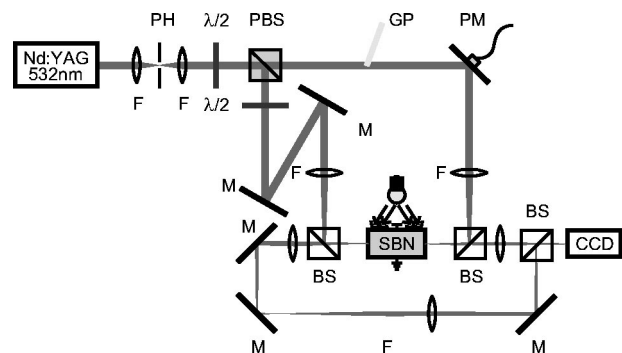


Fig. 1. Experimental setup for a CP dipole-mode vector soliton: PH, pinhole; F's, lenses;  $\lambda/2$ , half-wave plate; PBS, polarizing beam splitter; BSs, beam splitters; GP, glass plate; M's, mirrors; PM, piezo-driven mirror.

graphic  $c$  axis. To take advantage of the large  $r_{33}$  electro-optic coefficient of SBN, we polarized the beams along the same direction. Background illumination is achieved with a white-light source, which permits adjustment of the dark intensity. To be able to observe the two crystal faces simultaneously, we image both onto the same CCD camera. The optical dipole is generated by introduction of a tilted glass plate into one of the arms, a well-known technique for the creation of optical dipoles, and is oriented perpendicular to the  $c$  axis to minimize effects of photorefractive anisotropy.<sup>11</sup> To compensate for the beam bending mentioned above, the beams are launched into the crystal such that the input face of one beam coincides with the exit face of the CP beam propagating as an individual soliton. This results in a small angle ( $<1^\circ$ ) between the two incident beams. The power of the FM beam is  $P_{\text{FM-beam}} \approx 1.00 \mu\text{W}$ , and the power of the dipole is  $P_{\text{dipole}} \approx 1.35 \mu\text{W}$ . The approximate diameter of the beams at the input face is  $d \approx 20 \mu\text{m}$  FWHM. The geometry of the SBN crystal is  $23(a) \text{ mm} \times 5(b) \text{ mm} \times 5(c) \text{ mm}$ , and propagation is along the  $a$  axis of the crystal for maximum propagation length, corresponding to approximately four diffraction lengths. The external field was set to  $E_{\text{ext}} \approx 1.2 \text{ kV/cm}$ , and the background illumination was adjusted to permit stable self-focusing and soliton formation of the individually propagating FM beam.

The formation of the dipole-mode vector soliton is shown in Fig. 2. The images are taken at the exit face of the dipole beam. The less-intense spot in the middle of the images is the reflection of the FM input at the crystal face; it serves as a reference and does not influence soliton formation. When the nonlinearity is turned on, the dipole initially self-focuses to the left of the FM beam [Fig. 2(b)]. This is due to the initial angle between the beams. The dipole is then strongly deflected to the right, as beam bending and attraction from the FM soliton act in the same direction. The dipole splits, and two spots of low intensity with a much smaller separation appear on the left-hand side of the FM beam [Fig. 2(c)]. As time elapses, this trapped part of the dipole draws intensity from the nontrapped part and the nontrapped part is attracted horizontally toward the FM input [Fig. 2(d)]. After approximately 35 min the system reaches equilibrium, with almost all the power of the dipole trapped [Fig. 2(e)]. When the FM beam is blocked, the dipole components quickly repel and move to the right as a result of beam bending. Figure 2(f) shows the dipole after it has propagated individually for approximately 5 min. The separation of the dipole components of the trapped and the nontrapped parts in Fig. 2(e) was  $d_{\text{tr}} \approx 38$  and  $d_{\text{nontr}} \approx 87 \mu\text{m}$ , respectively, compared with  $d_{\text{indiv}} \approx 57 \mu\text{m}$  for the individually propagating dipole.

The transient formation dynamics differ significantly from those in the copropagating case, which makes them particularly interesting. The most striking fact is the splitting of the dipole into two parts, which is not observed in the copropagating geometry. Although at a quick glance such an effect might be attributed to a phenomenon such as conical scatter-

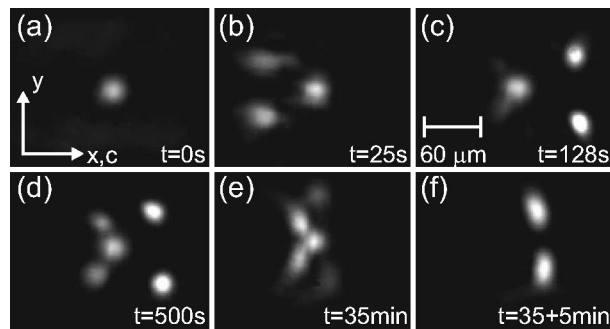


Fig. 2. Images of the dipole exit face of the crystal (the beam from the FM input face to the camera is blocked). In each figure the spot in the middle is the reflection of the FM input, serving as a reference. (a) Linear propagation. Soliton formation at times (b)  $t=25$  s (c)  $t=128$  s, and (d)  $t=500$  s after the nonlinearity has been turned on. (e) Stable state after  $t \approx 35$  min. (f) Individually propagating dipole approximately  $t=5$  min after the FM beam was blocked.

ing, a thorough analysis shows immediately that these effects can be excluded: The two interacting solitons are mutually incoherent and thereby are not able to interfere with each other. Moreover, the angles at which these new beams appear are in the range of  $1^\circ$ , much smaller than the scattering cone, which should be well above  $10^\circ$ . Instead, the split can be explained by the presence of an angle between the beams that is introduced to compensate for the effects of beam bending. Soliton formation in photorefractive crystals is a two-step process in which the beam self-focuses initially and then is displaced by beam bending.<sup>10</sup> After self-focusing of the CP beams but before beam bending takes place, the beams cross at only one point inside the crystal owing to the angular adjustment. At this point the colliding beams interact strongly, which causes the observed splitting. The nontrapped part of the dipole is then deflected by the combined forces of beam bending and incoherent attraction of the dipole, causing the dipole to overshoot. This explains why the nontrapped dipole part is initially displaced farther than the individually propagating dipole, which one can see by comparing Figs. 2(c) and 2(d) with Fig. 2(f). The second remarkable feature of the CP dipole is the long time scale of its formation. It differs significantly from that of copropagating solitons, with formation times in the range of 20–50 s or even less for higher intensities,<sup>10</sup> compared with  $\sim 30$  min for the CP dipole-mode vector soliton to reach a stable state for similar parameters. As can be seen from Figs. 2(c)–2(e), the trapped dipole is not aligned with the input of the CP beam but is displaced slightly to the left. The output of the FM beam, which can be seen in Fig. 3, shows a similar picture. The FM soliton is displaced to the left of the dipole input, in agreement with earlier simulations<sup>6</sup> that predicted a threshold propagation length at which the symmetry along the dipole axis is broken. Thus our experimental results are above this threshold length. Additionally, we observe that the FM beam splits as well. Figure 3(b) shows the exit face of the FM beam when the dipole

is blocked for a short moment. A fraction of the beam has split from the main part and has coupled into the dipole waveguide.

To verify our experimental results we carried out simulations in the anisotropic, nonlocal model.<sup>12</sup> The two CP beams are denoted by their slowly varying envelopes  $F$  and  $B$ . The total optical field can then be written as  $F \exp(ikz) + B \exp(-ikz)$ , where  $k$  is the wave vector in the undisturbed crystal. As we are considering  $F$  and  $B$  to be mutually incoherent, the total intensity is given by  $I = |F|^2 + |B|^2$ . The Kukhtarev model of the photorefractive crystal leads under simplifying but well-justified assumptions to the following equation:

$$\frac{\tau}{1+I} \partial_t \Delta \phi + \Delta \phi + \nabla \ln(1+I) \nabla \phi = E_{\text{ext}} \partial_x \ln(1+I) + \kappa \{ \Delta \ln(1+I) + [\nabla \ln(1+I)]^2 \} \quad (1)$$

for the potential  $\phi$  of the electrical screening field, which causes a nonlinear change of the refractive index by means of the Pockels effect.  $E_{\text{ext}}$  denotes the externally applied electrical field,  $\kappa = -k_B T / e$  is the diffusive coupling strength,  $\tau$  is the effective time constant of the crystal, and  $I$  is measured in units of background intensity.

The propagation of the beams is described in a paraxial approximation by the set of equations

$$\partial_z F - \frac{i}{2} \nabla_{\perp}^2 F + \frac{i}{2} \gamma (E_{\text{ext}} F - \partial_x \phi F) = 0, \quad (2a)$$

$$-\partial_z B - \frac{i}{2} \nabla_{\perp}^2 B + \frac{i}{2} \gamma (E_{\text{ext}} B - \partial_x \phi B) = 0, \quad (2b)$$

with nonlinear coupling constant  $\gamma = k^2 x_0^2 n_0^2 r_{\text{eff}}$ , which contains the refractive index of the unperturbed crys-

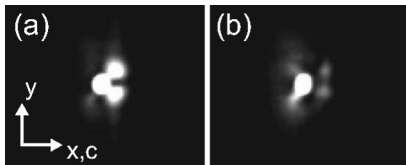


Fig. 3. Images of the dipole input face at steady state  $\approx 35$  min after the nonlinearity has been turned on. (a) The output of the FM beam is displaced to the left of the dipole input. (b) Output of the FM when the dipole is immediately blocked; a small fraction of the FM beam has coupled into the dipole waveguide.

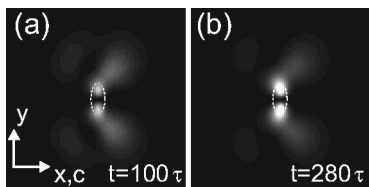


Fig. 4. Numerical simulations of the dipole-mode vector soliton. The images show the exit face of the dipole at (a)  $t = 100 \tau$  and (b)  $t = 280 \tau$  after the start of the simulation. The locations of the input beams are indicated by the dashed ellipses.

tal  $n_0$ , the effective element of the electro-optic tensor  $r_{\text{eff}}$ , and transverse scaling constant  $x_0$ .  $\nabla_{\perp}^2$  denotes the transverse Laplacian. The propagation ( $z$ ) axis is scaled to diffraction length  $L_D = kx_0^2$ . The values used in the simulations are  $x_0 = 10 \mu\text{m}$  (typical beam widths are approximately  $1 \dots 2 x_0$ ),  $r_{\text{eff}} = 280 \text{ pm/V}$ ,  $n_0 = 2.35$ ,  $E_{\text{ext}} = 2.5 \text{ kV/cm}$ , and  $k = 2\pi n_0 / \lambda$ , with  $\lambda = 532 \text{ nm}$ . The total propagation distance was chosen to be  $4L_D$  (11.1 mm).

The results of the simulations are shown in Fig. 4. Figures 4(a) and 4(b) show the exit face of the dipole beam at times  $t = 100 \tau$  and  $t = 280 \tau$ , respectively, after the start of the simulation. Although the numerical and experimental results differ in detail, the main features of the interaction are similar. The splitting of the dipole into a trapped and a nontrapped part can clearly be observed in Fig. 4(a), although it is not so pronounced as in the experiment. As time elapses, the trapped part grows in intensity, drawing energy from the nontrapped part [Fig. 4(b)]. The second main feature, the exceptionally long time scale, is reproduced as well, with the time constant  $\tau$  corresponding to approximately  $\tau \approx 15 \text{ s}$ .

To summarize, we have shown the existence of a stable counterpropagating dipole-mode vector soliton in a photorefractive SBN crystal. The vector soliton differs considerably in many aspects from its counterpart in copropagating geometry. The time scale of the transient dynamics is significantly larger. During the formation the beams split, and a trapped and a nontrapped part of the dipole can be observed.

J. Schröder's e-mail address is jschrod@uni-muenster.de.

## References

1. M. Haelterman, A. P. Sheppard, and A. W. Snyder, Opt. Commun. **103**, 145 (1993).
2. O. Cohen, R. Uzdin, T. Carmon, J. W. Fleischer, M. Segev, and S. Odoulov, Phys. Rev. Lett. **89**, 133901 (2002).
3. O. Cohen, S. Lan, T. Carmon, J. A. Giordmaine, and M. Segev, Opt. Lett. **27**, 2013 (2002).
4. C. Rotschild, O. Cohen, O. Manela, T. Carmon, and M. Segev, J. Opt. Soc. Am. B **21**, 1354 (2004).
5. M. Belić, P. Jander, A. Strinić, A. Desyatnikov, and C. Denz, Phys. Rev. E **68**, 025601(R) (2003).
6. K. Motzek, P. Jander, A. Desyatnikov, M. Belić, C. Denz, and F. Kaiser, Phys. Rev. E **68**, 066611 (2003).
7. W. Królikowski, E. A. Ostrovskaya, C. Weilnau, M. Geisser, G. McCarthy, Y. S. Kivshar, C. Denz, and B. Luther-Davies, Phys. Rev. Lett. **85**, 1424 (2000).
8. T. Carmon, C. Anastassiou, S. Lan, D. Kip, Z. H. Musslimani, and M. Segev, Opt. Lett. **25**, 1113 (2000).
9. J. J. Garcia-Ripoll, V. M. Perez-Garcia, E. A. Ostrovskaya, and Y. S. Kivshar, Phys. Rev. Lett. **85**, 82 (2000).
10. C. Denz, W. Królikowski, J. Petter, C. Weilnau, T. Tschudi, M. R. Belić, F. Kaiser, and A. Stepken, Phys. Rev. E **60**, 6222 (1999).
11. W. Królikowski, B. Luther-Davies, C. Denz, J. Petter, C. Weilnau, A. Stepken, and M. R. Belić, Appl. Phys. B **68**, 975 (1999).
12. A. A. Zozulya and D. Z. Anderson, Phys. Rev. A **51**, 1520 (1995).